Control Theory Tech, Vol. 18, No. 1, pp. 92–106, February 2020

Control Theory and Technology

http://link.springer.com/journal/11768

Stability analysis for time delay control of nonlinear systems in discrete-time domain with a standard discretisation method

Jinoh LEE [1*†], Gustavo A. MEDRANO-CERDA [1*], Je Hyung JUNG [2]

1.*Advanced Robotics, Istituto Italiano di Tecnologia, Via Morego 30, Genoa, 16163, Italy;*

2.*Tecnalia Research and Innovation, Mikeletegi Pasealekua, 1-3, E-20009, Donostia-San Sebastián, Spain*

Received 10 July 2019; revised 5 November 2019; accepted 11 December 2019

Abstract

This paper provides stability analysis results for discretised time delay control (TDC) as implemented in a sampled data system with the standard form of zero-order hold. We first substantiate stability issues in discrete-time TDC using an example and propose sufficient stability criteria in the sense of Lyapunov. Important parameters significantly affecting the overall system stability are the sampling period, the desired trajectory and the selection of the reference model dynamics.

Keywords: Time delay control (TDC), discretisation, stability analysis, zero-order hold

DOI https://doi.org/10.1007/s11768-020-9125-2

1 Introduction

Time-delay control (TDC) was first introduced in [1–4] and recognized as a promising technique in the robust control area. TDC exploits time-delayed information to estimate and cancel out unknown dynamics, unexpected disturbances and rendering the desired closed-loop dynamics into the plant. Owing to the simplicity of its structure, model-independence, and numerical efficiency, it has been successfully demonstrated to provide robust performance in diverse nonlinear control system applications [5–14].

A compact sufficient stability criterion regarding the gain of TDC was proven in [15, 16] based on the assumption of the continuous-time TDC and infinitesimal time delay. However, TDC is generally implemented in digital devices and the time delay is set to the sampling period of the control hardware, which is a constant during the control process. Henceforth, the aforementioned assumption fails to represent the actual sampled-data system stability behavior by ignoring the time delay be-

†Corresponding author.
E-mail: jinoh.lee@iit.it. Tel.: +39-10-2896-536.
*Co-First author.

ing equal to the sampling time interval.

A more realistic stability analysis was performed in [17, 18], which considers the sampled data system including the time delay, i.e., discrete-time version of TDC and nonlinear continuous system. However, the authors introduced a modified form of a zero order hold (ZOH) in their analysis and this is quite different from the standard ZOH implementation.

In this paper, we propose sufficient criteria based on Lyapunov stability theory, taking into account the actual impact on selecting the gain and sampling period under discrete-time TDC implemented with a standard ZOH. The paper contributions are presenting a formulation based on the standard zero order hold and carrying out a comparison between the stability results when using the standard zero order hold and a modified zero order hold considered in [17, 18].

In the rest of the paper, Section 2 briefly reviews TDC and substantiates the stability issue with examples. Section 3 proposes stability criteria, and the results are numerically verified in Section 4. The conclusion is finally drawn in Section 5.

2 Time delay control and its stability issues

2.1 TDC in continuous domain

Consider a nonlinear system of the form

$$\dot{x} = f(x) + g(x)u, \tag{1}$$

where $x = [x_1 \ \cdots \ x_n]^{\mathrm{T}} \in \mathbb{R}^n$ denotes the state vector, and $u = [u_1 \ \cdots \ u_p]^{\mathrm{T}} \in \mathbb{R}^p$ denotes the control input. Throughout the paper, we assume that $f(x)$ and $g(x)$ are smooth functions of the state vector x and consider the physical systems can be represented in phase variable form as follows [15]:

$$x = \begin{bmatrix} x_{\mathrm{q}} \\ x_p \end{bmatrix}, \quad f(x) = \begin{bmatrix} x_{\mathrm{s}} \\ f_p(x) \end{bmatrix}, \quad g(x) = \begin{bmatrix} \mathbf{0}_{\mathrm{s}} \\ g_p(x) \end{bmatrix}, \tag{2}$$

where $x_{\mathrm{q}} = [x_1 \ \cdots \ x_{n-p}]^{\mathrm{T}}, x_{\mathrm{s}} = [x_{p+1} \ \cdots \ x_n]^{\mathrm{T}} \in \mathbb{R}^{n-p}$; $x_p, f_p(x) \in \mathbb{R}^p$; $\mathbf{0}_{\mathrm{s}} \in \mathbb{R}^{(n-p)\times p}$ denotes a zero matrix and $g_p \in \mathbb{R}^{p\times p}$ is a non-singular matrix.

Remark 1 A large class of mechanical systems arising in robotics can be naturally expressed in phase variable form. More complex nonlinear systems, such as a multiple-link manipulator and robotic devices utilizing series elastic actuators, can be transformed into the phase variable form by successive differentiation with respect to time and expressing the results in terms of a single nonlinear differential equation. This is akin to input/output linearization procedures, where the output is differentiated with respect to time several times until at least one of the control inputs appears in the high order differential equation. Such systems are described in [16, 17] and [19, Chapter 13].

The desired closed-loop performance is specified by a stable reference model given by

$$\dot{x}_{\mathrm{m}} = A_{\mathrm{m}} x_{\mathrm{m}} + B_{\mathrm{m}} R, \tag{3}$$

where $x_{\mathrm{m}} \in \mathbb{R}^n$ denotes the reference model state vector, $R \in \mathbb{R}^p$ denotes the input vector of the reference model, $A_{\mathrm{m}} \in \mathbb{R}^{n\times n}$ denotes the system matrix which is constant and stable, and $B_{\mathrm{m}} \in \mathbb{R}^{n\times p}$ denotes the input distribution matrix.

The TDC law given in [15] is then written as follows:

$$u_{(t)} = u_{(t-\lambda)} + \bar{g}^{+}[-\dot{x}_{(t-\lambda)} + A_{\mathrm{m}} x_{(t)} + B_{\mathrm{m}} R_{(t)}], \tag{4}$$

where λ denotes the time delay, $\bar{g}^{+}$ denotes a pseudo-inverse of $\bar{g}$ defined by $\bar{g}^{+} \triangleq (\bar{g}^{\mathrm{T}}\bar{g})^{-1}\bar{g}^{\mathrm{T}}$ in which $\bar{g}$ is a constant matrix representing the known range of $g(x)$.

2.2 Problem statement of TDC stability in discrete domain

In [16], the well-known stability criteria of the closed-loop system using TDC (4) is derived based on input-output linearisation of (1) as the following sufficient condition:

$$\|I_p - g_p(x)\bar{g}_p^{-1}\| < 1, \tag{5}$$

where $I_p \in \mathbb{R}^{p\times p}$ denotes the identity matrix, and $\bar{g}_p$ is a constant matrix.

The above stability condition is based on the assumption: the time delay $\lambda \to 0$ in continuous time domain. However, the TDC is originally intended for digital control and the time delay λ is set to be equal to the sampling period T in the implemented digital device. As a result, the closed-loop system forms a sampled-data system. Although the stability condition (5) is compact in form and practical with sufficiently fast sampling period, it is the fact that the time-delay λ is a crucial factor affecting the closed-loop system stability [17, 18].

In this light, the authors in [17, 18] proposed a more accurate stability criterion including not only g but also λ of the realistic sampled-data system, i.e., discrete-time TDC and a nonlinear continuous-time system. However, the nonlinear continuous-time closed-loop system is approximated by a discrete-time model with a particular form of ZOH in a way such that

$$x_{(k+1)} = h(x_{(k)}, u_{(k+1)}) \text{ or } x_{(k)} = h(x_{(k-1)}, u_{(k)}), \quad (6)$$

and in [17,18], a modified discrete-time TDC controller is also introduced as follows:

$$\boldsymbol{u}_{(k)} = \boldsymbol{u}_{(k-1)} + \bar{g}^{+}[-\dot{\boldsymbol{x}}_{(k-1)} + \underbrace{\boldsymbol{A}_{\mathrm{m}}\boldsymbol{x}_{(k-1)} + \boldsymbol{B}_{\mathrm{m}}\boldsymbol{R}_{(k-1)}}_{\substack{\text{Additional delay} \\ \text{using the modified ZOH}}}], \quad (7)$$

where k denotes the kth sample and h denotes a nonlinear function with the state x and the input u. For brevity of expression, (6) is hereinafter referred to as the modified ZOH. This simplifies the stability analysis for the modified discrete-time TDC.

In contrast, the standard ZOH discretisation of (4) gives

$$x_{(k+1)} = h(x_{(k)}, u_{(k)}) \text{ or } x_{(k)} = h(x_{(k-1)}, u_{(k-1)}), \quad (8)$$

and the corresponding TDC implementation [5–14] is

$$\boldsymbol{u}_{(k)} = \boldsymbol{u}_{(k-1)} + \bar{g}^{+}[-\dot{\boldsymbol{x}}_{(k-1)} + \underbrace{\boldsymbol{A}_{\mathrm{m}}\boldsymbol{x}_{(k)} + \boldsymbol{B}_{\mathrm{m}}\boldsymbol{R}_{(k)}}_{\substack{\text{No additional delay} \\ \text{using the standard ZOH}}} \quad (9)$$

One can observe that the discrete-time TDC with the modified ZOH, (7), introduces an additional delay compared with the standard form (9).

Note that in some computing software, particularly Simulink® in this paper, the zero order hold discretisation of a continuous time generates a continuous input signal $\boldsymbol{u}_{(t)}$ by holding each sample value $\boldsymbol{u}_{(k)}$ constant over one sampling time interval T, i.e., $\boldsymbol{u}_{(t)} = \boldsymbol{u}_{(k)}$ for $kT \leqslant t < (k+1)T$. Therefore, if the nonlinear continuous time is represented in Simulink® integrated with Matlab® and then sampled with the ZOH block in Simulink®, the corresponding sampled nonlinear model is of the form in (8) rather than (6).

Hence, the stability criterion for modified TDC and ZOH in [17,18] indeed is not applicable to standard implementation of TDC and ZOH (See the example in the following Section 2.3), and there is still a need to perform the stability analysis in the sense of the standard discrete-time TDC (8) and (9).

2.3 Examples on the problem of discrete TDC stability

To illustrate the basic ideas on how the discretisation methods impact on the stability analysis, a linearized model of the simple nonlinear system $\dot{x}_{(t)} = x^3_{(t)} + \sin x_{(t)} + 5u_{(t)}$ around zero is used as follows:

$$\dot{x}_{(t)} = x_{(t)} + 5u_{(t)}. \quad (10)$$

Here we consider three different implementations of the discrete-time TDC. In this case, $g_p(x)$ is a constant value, but unknown to the control designer. Therefore TDC controller gain has to be properly chosen as suggested by (5) [16]. Since this is the same example used in [17], one can easily analyse the impact of the discretisation methods comparing with the stability criterion proposed in [17].

Case 1 The standard discrete-time TDC (9) is applied to the system discretised by the standard ZOH (8).

Case 2 The modified discrete-time TDC (7) is applied to the system discretised by the modified ZOH [17].

Case 3 The modified discrete-time TDC is applied to the system discretised by the standard ZOH (6).

For the first case, a discrete-time system is sampled every T seconds with the standard form of ZOH, (8), as follows:

$$x_{(k)} = ax_{(k-1)} + bu_{(k-1)}, \quad (11)$$

where a and b are parameters determined by the sampling period. The standard discrete-time TDC is given with a reference model $A_{\mathrm{m}} = -40$ and a zero reference signal as

$$\begin{aligned} u_{(k)} &= u_{(k-1)} + \bar{g}^{-1}[-40x_{(k)} - \dot{x}_{(k-1)}] \\ &= u_{(k-1)} + \bar{g}^{-1}[-40x_{(k)} - 5u_{(k-1)} - x_{(k-1)}], \end{aligned} \quad (12)$$

where $\bar{g}$ is a suitably chosen scalar gain. The state space form of (11) and (12) is written as

$$\begin{bmatrix} 1 & 0 \\ \dfrac{40}{\bar{g}} & 1 \end{bmatrix} \begin{bmatrix} x_{(k)} \\ u_{(k)} \end{bmatrix} = \begin{bmatrix} a & b \\ -\dfrac{1}{\bar{g}} & 1 - \dfrac{5}{\bar{g}} \end{bmatrix} \begin{bmatrix} x_{(k-1)} \\ u_{(k-1)} \end{bmatrix}. \quad (13)$$

The closed-loop poles are therefore the eigenvalues of

$$\begin{bmatrix} 1 & 0 \\ -\dfrac{40}{\bar{g}} & 1 \end{bmatrix} \begin{bmatrix} a & b \\ -\dfrac{1}{\bar{g}} & 1 - \dfrac{5}{\bar{g}} \end{bmatrix}. \quad (14)$$

For the second case, a delay is introduced in the controller (12). It is then expressed as the following modified discrete-time TDC:

$$\begin{aligned} u_{(k)} =& u_{(k-1)} + \bar{g}^{-1}[-40x_{(k-1)} - \dot{x}_{(k-1)}] \\ =& u_{(k-1)} + \bar{g}^{-1}[-40x_{(k-1)} - 5u_{(k-1)} - x_{(k-1)}]. \end{aligned} \tag{15}$$

In this case, the state-space form of (11) and (15) is given as

$$\begin{bmatrix} x_{(k)} \\ u_{(k)} \end{bmatrix} = \begin{bmatrix} a & b \\ -\dfrac{40+1}{\bar{g}} & 1-\dfrac{5}{\bar{g}} \end{bmatrix} \begin{bmatrix} x_{(k-1)} \\ u_{(k-1)} \end{bmatrix}, \tag{16}$$

and the closed-loop poles are the eigenvalues of the followings:

$$\begin{bmatrix} a & b \\ -\dfrac{(40+1)}{\bar{g}} & 1-\dfrac{5}{\bar{g}} \end{bmatrix}. \tag{17}$$

The last case is that one uses the convention in [17]; the system is then discretised by the standard ZOH as

$$x_{(k)} = ax_{(k-1)} + bu_{(k)}, \tag{18}$$

while the discrete-time TDC is given by the modified form as (15). Writing this in state space form yields

$$\begin{bmatrix} 1 & -b \\ 0 & 1 \end{bmatrix} \begin{bmatrix} x_{(k)} \\ u_{(k)} \end{bmatrix} = \begin{bmatrix} a & 0 \\ -\dfrac{(40+1)}{\bar{g}} & 1-\dfrac{5}{\bar{g}} \end{bmatrix} \begin{bmatrix} x_{(k-1)} \\ u_{(k-1)} \end{bmatrix}. \tag{19}$$

The closed-loop poles are the eigenvalues of

$$\begin{bmatrix} 1 & b \\ 0 & 1 \end{bmatrix} \begin{bmatrix} a & b \\ -\dfrac{40+1}{\bar{g}} & 1-\dfrac{5}{\bar{g}} \end{bmatrix}. \tag{20}$$

Let $T = 0.01$ s. The parameters in the discrete-time system are then given as $a = 1.0101$ and $b = 0.0503$. Computing the eigenvalues for the three cases (14), (17), and (20), we can find the range of gains for which the closed-loop eigenvalues are inside the unit circle:

- for Case 1, (14), $2.9875 < \bar{g} < 497.1$;
- for Case 2, (17), $1.9876 < \bar{g} < 296.3$; and
- for Case 3, (20), $3.0125 < \bar{g} < 502.3$.

This example shows that the stability regions can be quite different using the standard or the modified ZOH analysis, even though the system is very simple as $g(x)$ is constant. The differences may become more significant in systems with increasing complexity. Also note that in (6), there is a direct connection between the input and the state (i.e., the transfer function is not strictly proper) and this cannot happen when sampling with the ZOHs. Therefore, it can be deduced that the stability analysis of the standard implementation of TDC—the case 1 with (8) and (9)—is still needed which has not been considered in previous publications.

3 Stability of standard discrete-time TDC

In this section, the closed-loop system stability is analysed for the standard form of the discrete-time TDC (9). The nonlinear continuous system is first discretised to obtain an approximate discrete-time model in a similar manner to [17], while the standard ZOH (8) is employed in this paper; the approximate discrete-time model of the closed-loop system is then derived under the standard discrete-time TDC, and sufficient conditions for the closed-loop system stability and tracking error performance are derived. Note that we strive to have consistent notation as introduced in [17] facilitating comparison between our work and previous results in [17,18].

3.1 Approximate discrete-time model

3.1.1 Nonlinear continuous time system discretization

Here we consider the standard ZOH (8) to discretise the nonlinear continuous-time system (1). In this sampled-data system, the control input will be a piecewise constant signal, $\boldsymbol{u}_{(t)} = \boldsymbol{u}_{(k-1)T} = \boldsymbol{u}_{(k-1)}$ for all t in the interval $[(k-1)T, kT)$, where $T > 0$ is a sampling time interval. However, the state $\boldsymbol{x}_{(k)}$ keeps on varying during its sampling interval between $(k-1)$ and k.

Suppose the sampling time interval T is divided into ϱ subintervals. The Euler approximation then gives the following difference equation:

$$\chi_{i+1} = \chi_i + \frac{T}{\varrho}[f(\chi_i) + g(\chi_i)\boldsymbol{u}_{(k-1)}], \tag{21}$$

where $i = 0, \dots, (\varrho - 1)$ denote the intermediate steps between the sampling intervals $(k-1)$ and k, $\chi_0 = \boldsymbol{x}_{(k-1)}$ and $\chi_\varrho = \boldsymbol{x}_{(k)}$. After applying Taylor series expansion [20] to the terms $f(\chi_i)$ and $g(\chi_i)\boldsymbol{u}_{(k-1)}$, we can write

$$\chi_{i+1} = (\boldsymbol{I}_n + \frac{T}{\varrho}\boldsymbol{H}_{(k-1)})\chi_i - \frac{T}{\varrho}\boldsymbol{H}_{(k-1)}\chi_0$$

$$+\frac{T}{\varrho}[f(\chi_0)+g(\chi_0)u_{(k-1)}], \tag{22}$$

where $H_{(k-1)} = F(\chi_0) + G(\chi_0, u_{(k-1)})$. See Appendix A for the detailed derivation using the Taylor series expansion.

From (22), we can write

$$\chi_\varrho = \chi_0 + \frac{T}{\varrho}\sum_{i=0}^{\varrho-1}(I_n + \frac{T}{\varrho}H_{(k-1)})^i[f(\chi_0)+g(\chi_0)u_{(k-1)}]. \tag{23}$$

Taking limits as $\varrho \to \infty$, equation (23) yields

$$x_{(k)} = \chi_0 + \int_0^T \lim_{i\to\infty}(I_n + \frac{t}{i}H_{(k-1)})^i \mathrm{d}t \times [f(\chi_0)+g(\chi_0)u_{(k-1)}], \tag{24}$$

Using the fact [21],

$$e^{t\times H_{(k-1)}} = \lim_{i\to\infty}[I_n + \frac{t}{i}\times H_{(k-1)}]^i,$$

the approximate discrete-time model of the nonlinear continuous system is then obtained as follows:

$$x_{(k)} = x_{(k-1)} + C_{(k-1)}[f(x_{(k-1)}) + g(x_{(k-1)})u_{(k-1)}], \tag{25}$$

where $C_{(k-1)} \triangleq \int_0^T e^{t\times H_{(k-1)}}\mathrm{d}t$. Note that if $H_{(k-1)}$ is invertible,

$$C_{(k-1)} = (e^{T\times H_{(k-1)}} - I_n)H_{(k-1)}^{-1}. \tag{26}$$

Remark 2 $C_{(k-1)}$ can be computed in Matlab® with reasonable accuracy. Another alternative is using a finite Taylor series expansion of the matrix exponential and then if needed carry out the integration numerically or using (26) when $H_{(k-1)}$ is invertible.

3.1.2 Closed-loop system under standard TDC

This section derives difference equations for the closed-loop errors. Such equations are the basis for the stability analysis. The closed-loop errors are defined as

$$e_{1(k)} \triangleq x_{(k)} - x_{\mathrm{m}(k)} \text{ and } e_{2(k)} \triangleq \frac{u_{(k)} - u_{\mathrm{m}(k)}}{k_\mathrm{s}}, \tag{27}$$

where $k_\mathrm{s} > 0$ denotes a scaling factor which adjusts the size of $u_{(k)} - u_{\mathrm{m}(k)}$ letting the tracking error $e_{1(k)}$ become significant in the overall stability analysis.

Consider the differential equation (1) evaluated at $(k-1)T$ as $\dot{x}_{(k-1)} = f_{(k-1)} + g_{(k-1)}u_{(k-1)}$, where $f_{(k-1)} \triangleq f(x_{(k-1)})$ and $g_{(k-1)} \triangleq g(x_{(k-1)})$ are used to simplify notation. The standard discrete-time TDC (9) is rewritten as follows:

$$u_{(k)} = \bar{g}^+[(\bar{g} - g_{(k-1)})u_{(k-1)} - f_{(k-1)} + A_\mathrm{m}x_{(k)} + B_\mathrm{m}R_{(k)}]. \tag{28}$$

Applying (28) to (25) forms the closed-loop system as

$$x_{(k+1)} = x_{(k)} + C_k[f_k + g_k\bar{g}^+(\bar{g} - g_{(k-1)})u_{(k-1)}] + C_kg_k\bar{g}^+[-f_{(k-1)} + A_\mathrm{m}x_{(k)} + B_\mathrm{m}R_{(k)}]. \tag{29}$$

In (29), f_k can be expressed in the following form by Taylor series expansion around $x_{\mathrm{m}(k)}$ [20]:

$$f_k = f(x_{\mathrm{m}(k)}) + F(x_{\mathrm{m}(k)})[x_{(k)} - x_{\mathrm{m}(k)}] + O_1(x_{(k)}, x_{\mathrm{m}(k)}), \tag{30}$$

where $F \in \mathbb{R}^{n\times n}$ is defined in Appendix A and $O_1(x_{(k)}, x_{\mathrm{m}(k)}) \in \mathbb{R}^n$ denotes the residual term of the first order Taylor series expansion detailed in Appendix B. Hereinafter, for brevity, $O_1(x_{(k)}, x_{\mathrm{m}(k)})$ is written as $O_{1(k)}$.

An input vector of the reference model is defined as

$$u_{\mathrm{m}(k)} \triangleq \bar{g}^+\{[\bar{g} - g(x_{\mathrm{m}(k-1)})]u_{\mathrm{m}(k-1)} - f(x_{\mathrm{m}(k-1)}) + A_\mathrm{m}x_{\mathrm{m}(k)} + B_\mathrm{m}R_{(k)}\}. \tag{31}$$

Note that $u_{\mathrm{m}(k)}$ may not be unique; in this paper, it is defined to be in a consistent format as that for $u_{(k)}$ in (28), which is different from the one defined in [17,18]. Then, discretising the reference model (3) using the standard ZOH gives

$$x_{\mathrm{m}(k+1)} = D_1x_{\mathrm{m}(k)} + (D_1 - I)A_\mathrm{m}^{-1}B_\mathrm{m}R_{(k)}, \tag{32}$$

where $D_1 = e^{TA_\mathrm{m}}$.

In phase variable form, we can write the following identity [15]:

$$(I - \bar{g}\bar{g}^+)[-f_k + A_\mathrm{m}x_{(k)} + B_\mathrm{m}R_{(k)}] = 0. \tag{33}$$

From (28), one can obtain

$$\bar{g}^+[A_\mathrm{m}x_{(k)} + B_\mathrm{m}R_{(k)}] = u_{(k)} + \bar{g}^+(g_{(k-1)} - \bar{g})u_{(k-1)} + \bar{g}^+f_{(k-1)}. \tag{34}$$

Using (33) and (34),

$$B_\mathrm{m}R_{(k)} = (I - \bar{g}\bar{g}^+)f_k + \bar{g}\bar{g}^+f_{(k-1)} + \bar{g}u_{(k)} + \bar{g}\bar{g}^+(g_{(k-1)} - \bar{g})u_{(k-1)} - A_\mathrm{m}x_{(k)}. \tag{35}$$

Note that (33)–(35) hold for $x_{\mathrm{m}(k)}$ in place of $x_{(k)}$.

Finally, using (28)–(35), we can express the closed-loop errors as follows:

$$\begin{aligned} e_{1(k+1)} =& S_1 e_{1(k)} + S_2 e_{1(k-1)} + S_3 e_{2(k-1)} \\ &+ Q_1 O_{1(k)} + Q_2 O_{1(k-1)} \\ &+ Q_3 f(x_{\mathrm{m}(k)}) + Q_4 f(x_{\mathrm{m}(k-1)}) \\ &+ Q_5 u_{\mathrm{m}(k)} + Q_6 u_{\mathrm{m}(k-1)}, \end{aligned} \tag{36}$$

$$\begin{aligned} e_{2(k+1)} =& -E_1 e_{1(k+1)} + S_4 e_{1(k)} + S_5 e_{2(k)} \\ &+ Q_7 O_{1(k)} + Q_8 u_{\mathrm{m}(k)}. \end{aligned} \tag{37}$$

The detailed expression for the matrices $S_{1,\dots,5}$, $Q_{1,\dots,8}$, and E_1 are provided in Appendix C. From (36) and (37), we have

$$\underbrace{\begin{bmatrix} I_n & 0_{n\times p} & 0_n & 0_{n\times p} \\ E_1 & I_p & 0_{p\times n} & 0_p \\ 0_n & 0_{n\times p} & I_n & 0_{n\times p} \\ 0_{p\times n} & 0_p & 0_{p\times n} & I_p \end{bmatrix}}_{E} \begin{bmatrix} e_{1(k+1)} \\ e_{2(k+1)} \\ e_{1(k)} \\ e_{2(k)} \end{bmatrix} = \underbrace{\begin{bmatrix} S_1 & 0_{n\times p} & S_2 & S_3 \\ S_4 & S_5 & 0_{p\times n} & 0_p \\ I_n & 0_{n\times p} & 0_n & 0_{n\times p} \\ 0_{p\times n} & I_p & 0_{p\times n} & 0_p \end{bmatrix}}_{S_k} \begin{bmatrix} e_{1(k)} \\ e_{2(k)} \\ e_{1(k-1)} \\ e_{2(k-1)} \end{bmatrix} + \underbrace{\begin{bmatrix} Q_{1k} \\ Q_{2k} \\ 0_{n\times 1} \\ 0_{p\times 1} \end{bmatrix}}_{Q_k}, \tag{38}$$

where

$$\begin{aligned} \begin{bmatrix} Q_{1k} \\ Q_{2k} \end{bmatrix} \triangleq& \begin{bmatrix} Q_1 \\ Q_7 \end{bmatrix} O_{1(k)} + \begin{bmatrix} Q_2 \\ 0_{p\times 1} \end{bmatrix} O_{1(k-1)} \\ &+ \begin{bmatrix} Q_3 \\ 0_{p\times 1} \end{bmatrix} F(x_{\mathrm{m}(k)}) + \begin{bmatrix} Q_4 \\ 0_{p\times 1} \end{bmatrix} F(x_{\mathrm{m}(k-1)}) \\ &+ \begin{bmatrix} Q_5 \\ Q_8 \end{bmatrix} u_{\mathrm{m}(k)} + \begin{bmatrix} Q_6 \\ 0_{p\times 1} \end{bmatrix} u_{\mathrm{m}(k-1)}. \end{aligned}$$

Hence, from (38) and the following state vector

$$e_{(k)} \triangleq [e_{1(k)}^{\mathrm{T}} \;\; e_{2(k)}^{\mathrm{T}} \;\; e_{1(k-1)}^{\mathrm{T}} \;\; e_{2(k-1)}^{\mathrm{T}}]^{\mathrm{T}},$$

the approximate discrete-time closed-loop error under the standard discrete-time TDC satisfies the difference equation

$$e_{(k+1)} = E^{-1} S_k e_{(k)} + E^{-1} Q_k, \tag{39}$$

or equivalently,

$$e_{(k+1)} = M_k e_{(k)} + N_k \triangleq E_{\mathrm{CL}}^{\mathrm{a}}(e_{(k)}), \tag{40}$$

where $M_k \triangleq (E^{-1} S_k)$ and $N_k \triangleq (E^{-1} Q_k)$.

Note that the implementation of the controller does not require knowledge of the nonlinear functions (see equations (4), (7) and (9)). This is why TDC is an appealing strategy. However the stability analysis requires some knowledge about the nonlinear functions $f(x)$ and $g(x)$, for example using nominal or estimated models. Uncertainty can be incorporated in the stability analysis by introducing perturbations as described in [15].

Remark 3 The use of the approximate discrete-time model for the entire stability analysis is confirmed to be valid by the consistency property of the approximate and exact closed-loop discrete-time model proven in [17, 22].

3.2 Stability analysis and sufficient conditions

This section aims at deriving sufficient conditions for the closed-loop system stability of the standard discrete-time TDC. For the analysis, we first consider the time varying homogeneous difference equation of (40) given as

$$e_{(k+1)} = M_k e_{(k)}. \tag{41}$$

Lemma 1 Define the largest singular value of all M_k's as

$$\xi \triangleq \max_k \|M_k\|. \tag{42}$$

If ξ satisfies

$$0 < \xi < 1, \tag{43}$$

then the nominal close-loop model (41) is asymptotically stable and there exist positive definite real symmetric matrices $P = \alpha I$, where α is any positive scalar, such that $V(e_{(k)}) = e_{(k)}^{\mathrm{T}} P e_{(k)}$ is a positive scalar function satisfying

$$b_1 \|e_{(k)}\|^2 \leqslant V(e_{(k)}) \leqslant b_2 \|e_{(k)}\|^2, \tag{44}$$

$$\Delta V(e_{(k)}) = V(e_{(k+1)}) - V(e_{(k)}) \leqslant -b_3 \|e_{(k)}\|^2, \tag{45}$$

where b_1, b_2, and b_3 are positive constants for all k. For $P = \alpha I$, $b_1 = b_2 = \alpha$ and $b_3 = \alpha(1 - \xi^2)$.

Proof Asymptotic stability follows from (41) and (43), since M_k is a contraction mapping $\|e_{(k)}\| \leqslant \xi^{(k-k_0)} \|e_{(k_0)}\|$. Given that P is a positive definite real symmetric matrix, we have

$$\lambda_{\min}(P) \|e_{(k)}\|^2 \leqslant V(e_{(k)}) \leqslant \lambda_{\max}(P) \|e_{(k)}\|^2,$$

where $\lambda_{\min}(\boldsymbol{P})$ and $\lambda_{\max}(\boldsymbol{P})$ denote, respectively, the minimum and maximum eigenvalues of the constant positive definite real symmetric matrix, $\boldsymbol{P}$, and therefore these are positive constants, $b_1 = \lambda_{\min}(\boldsymbol{P})$ and $b_2 = \lambda_{\max}(\boldsymbol{P})$; and (44) is established.

Now let us prove that $V(\boldsymbol{e}_{(k)})$ satisfies (45) for $\xi < 1$. Using (41), we obtain $\Delta V(\boldsymbol{e}_{(k)})$ as follows:

$$\begin{aligned}\Delta V(\boldsymbol{e}_{(k)}) =& V(\boldsymbol{e}_{(k+1)}) - V(\boldsymbol{e}_{(k)}) = \boldsymbol{e}_{(k)}^{\mathrm{T}}(\boldsymbol{M}_k^{\mathrm{T}}\boldsymbol{P}\boldsymbol{M}_k - \boldsymbol{P})\boldsymbol{e}_{(k)}\\ =& -\boldsymbol{e}_{(k)}^{\mathrm{T}}(\boldsymbol{P} - \boldsymbol{M}_k^{\mathrm{T}}\boldsymbol{P}\boldsymbol{M}_k)\boldsymbol{e}_{(k)},\\ \Delta V(\boldsymbol{e}_{(k)}) \leqslant& -\lambda_{\min}(\boldsymbol{P} - \boldsymbol{M}_k^{\mathrm{T}}\boldsymbol{P}\boldsymbol{M}_k)\|\boldsymbol{e}_{(k)}\|^2 \leqslant -b_3\|\boldsymbol{e}_{(k)}\|^2,\end{aligned}$$

where $0 < b_3 \leqslant \min_k[\lambda_{\min}(\boldsymbol{P} - \boldsymbol{M}_k^{\mathrm{T}}\boldsymbol{P}\boldsymbol{M}_k)]$.

Finally for $\boldsymbol{P} = \alpha\boldsymbol{I}$, $\lambda_{\min}(\boldsymbol{P}) = \lambda_{\max}(\boldsymbol{P}) = \alpha$ and we have

$$\begin{aligned}\lambda_{\min}(\boldsymbol{P} - \boldsymbol{M}_k^{\mathrm{T}}\boldsymbol{P}\boldsymbol{M}_k) &= \alpha\lambda_{\min}(\boldsymbol{I} - \boldsymbol{M}_k^{\mathrm{T}}\boldsymbol{M}_k)\\ &\leqslant \alpha(1 - \lambda_{\max}(\boldsymbol{M}_k^{\mathrm{T}}\boldsymbol{M}_k))\\ &\leqslant \alpha(1 - \xi^2).\end{aligned}$$

Here we have used two facts: the eigenvalues of $(\boldsymbol{I} - \boldsymbol{M}_k^{\mathrm{T}}\boldsymbol{M}_k)$ are given by $(1 - \lambda(\boldsymbol{M}_k^{\mathrm{T}}\boldsymbol{M}_k))$ and $\lambda_{\max}(\boldsymbol{M}_k^{\mathrm{T}}\boldsymbol{M}_k) = \sigma_{\max}^2(\boldsymbol{M}_k) = \|\boldsymbol{M}_k\|^2$, where $\sigma_{\max}(\boldsymbol{M}_k)$ denotes the largest singular value of $\boldsymbol{M}_k$. Hence when $\boldsymbol{P} = \alpha\boldsymbol{I}$, we have $b_1 = b_2 = \alpha$ and $b_3 = \alpha(1 - \xi^2)$.

This completes the proof of Lemma 1. □

We point out the proof of Lemma 1 is evaluated using the states of the approximate model. Also note that suitable positive matrices $\boldsymbol{P}$ exist besides $\boldsymbol{P} = \alpha\boldsymbol{I}$, yet $\boldsymbol{P}$ is not an arbitrary symmetric positive definite matrix. To determine such matrices a set of linear matrix inequalities (LMIs), $(\boldsymbol{P} - \boldsymbol{M}_k^{\mathrm{T}}\boldsymbol{P}\boldsymbol{M}_k) > 0$, can be solved. However solving LMIs becomes computationally expensive, particularly as both k and the size of $\boldsymbol{M}_k$ increase. Nevertheless we have given equations (44)–(45) in the most general terms so that in future developments we can visualise the effects of the positive scalars b_1, b_2 and b_3.

Lemma 2 [17] Consider the approximate closed-loop discrete-time model (40) as $\boldsymbol{E}_{\mathrm{CL}}^{\mathrm{a}}(\boldsymbol{e}_{(k)})$ and the exact closed-loop discrete-time model of (1) under discrete-time TDC as $\boldsymbol{E}_{\mathrm{CL}}^{\mathrm{e}}(\boldsymbol{e}_{(k)})$. Let $\boldsymbol{e} \in \mathbb{U}$ for each compact set $\mathbb{U} \subset \mathbb{R}^{n+p}$ and supposed that there exists a constant ϕ_1. Then, there exists a sampling time interval T^* such that $\forall T \in (0, T^*)$

$$\|\boldsymbol{E}_{\mathrm{CL}}^{\mathrm{e}}(\boldsymbol{e}_{(k)}) - \boldsymbol{E}_{\mathrm{CL}}^{\mathrm{a}}(\boldsymbol{e}_{(k)})\| \leqslant T \times \rho(T) \leqslant \phi_1, \tag{46}$$

where $\rho(T)$ belongs to class K_∞.

Theorem 1 Suppose $\boldsymbol{E}_{\mathrm{CL}}^{\mathrm{e}}(\boldsymbol{e}_{(k)})$ is the exact closed-loop discrete-time model and define $D_\delta = \{\boldsymbol{e}\,|\,\|\boldsymbol{e}\| \leqslant \delta\}$, where δ is a bound on the error norm. Let $V(\boldsymbol{e}_{(k)})$ be a Lyapunov function for the nominal system (41) satisfying (44) and (45) in Lemma 1. Taking a sufficiently large δ such that for all $\boldsymbol{e} \in D_\delta$, $\boldsymbol{N}_k$ in (40) and ϕ_1 of (46) in Lemma 2, then

$$\max_k\|\boldsymbol{N}_k\| + \phi_1 < (b_3/b_5)\sqrt{(b_1/b_2)}\nu\delta, \tag{47}$$

$$\omega \triangleq \max_k\|\boldsymbol{N}_k\| + \phi_1 - (b_3/b_5)\sqrt{(b_1/b_2)}\nu\delta < 0, \tag{48}$$

where $b_5 = \lambda_{\max}(\boldsymbol{P})\xi + \sqrt{\lambda_{\max}^2(\boldsymbol{P})\xi^2 + \lambda_{\max}(\boldsymbol{P})\nu b_3}$ and $0 < \nu < 1$, then for all

$$\|\boldsymbol{e}_{(k_0)}\| \leqslant \sqrt{(b_1/b_2)}\delta, \tag{49}$$

the solution to $\boldsymbol{E}_{\mathrm{CL}}^{\mathrm{e}}(\boldsymbol{e}_{(k)})$ satisfies

$$\|\boldsymbol{e}_{(k)}\| \leqslant C_2 e^{-\varphi(k-k_0)}\|\boldsymbol{e}_{(k_0)}\|,\ \ k_0 \leqslant \forall k < k_1, \tag{50}$$

and

$$\|\boldsymbol{e}_{(k)}\| \leqslant B,\ \ \forall k \geqslant k_1, \tag{51}$$

for $k_1 < \infty$, where $C_2 = \sqrt{\dfrac{b_2}{b_1}}$, $\varphi = (1-\nu)\dfrac{b_3}{2b_2}$, and $B = \dfrac{b_5}{b_3}C_2\dfrac{\max_k\|\boldsymbol{N}_k\| + \phi_1}{\nu}$.

Proof The difference $\Delta V(\boldsymbol{e}_{(k)}) = V(\boldsymbol{e}_{(k+1)}) - V(\boldsymbol{e}_{(k)})$ along the trajectory of $\boldsymbol{E}_{\mathrm{CL}}^{\mathrm{e}}(\boldsymbol{e}_{(k)})$ satisfies $\Delta V(\boldsymbol{e}_{(k)}) = \boldsymbol{E}_{\mathrm{CL}}^{\mathrm{eT}}(\boldsymbol{e}_{(k)})\boldsymbol{P}\boldsymbol{E}_{\mathrm{CL}}^{\mathrm{e}}(\boldsymbol{e}_{(k)}) - \boldsymbol{e}_{(k)}^{\mathrm{T}}\boldsymbol{P}\boldsymbol{e}_{(k)}$ and writing

$$\begin{aligned}\boldsymbol{E}_{\mathrm{CL}}^{\mathrm{e}}(\boldsymbol{e}_{(k)}) &= \boldsymbol{E}_{\mathrm{CL}}^{\mathrm{a}}(\boldsymbol{e}_{(k)}) + \boldsymbol{E}_{\mathrm{CL}}^{\mathrm{e}}(\boldsymbol{e}_{(k)}) - \boldsymbol{E}_{\mathrm{CL}}^{\mathrm{a}}(\boldsymbol{e}_{(k)})\\ &= (\boldsymbol{M}_k\boldsymbol{e}_{(k)} + \boldsymbol{N}_k) + \boldsymbol{E}_{\mathrm{CL}}^{\mathrm{e}}(\boldsymbol{e}_{(k)}) - \boldsymbol{E}_{\mathrm{CL}}^{\mathrm{a}}(\boldsymbol{e}_{(k)}),\end{aligned}$$

we then have

$$\begin{aligned}\Delta V(\boldsymbol{e}_{(k)}) =& \boldsymbol{e}_{(k)}^{\mathrm{T}}(\boldsymbol{M}_k^{\mathrm{T}}\boldsymbol{P}\boldsymbol{M}_k - \boldsymbol{P})\boldsymbol{e}_{(k)} + 2\boldsymbol{e}_{(k)}^{\mathrm{T}}\boldsymbol{M}_k^{\mathrm{T}}\boldsymbol{P}\boldsymbol{N}_k\\ &+\boldsymbol{N}_k^{\mathrm{T}}\boldsymbol{P}\boldsymbol{N}_k + 2\boldsymbol{N}_k^{\mathrm{T}}\boldsymbol{P}[\boldsymbol{E}_{\mathrm{CL}}^{\mathrm{e}}(\boldsymbol{e}_{(k)}) - \boldsymbol{E}_{\mathrm{CL}}^{\mathrm{a}}(\boldsymbol{e}_{(k)})]\\ &+[\boldsymbol{E}_{\mathrm{CL}}^{\mathrm{e}}(\boldsymbol{e}_{(k)}) - \boldsymbol{E}_{\mathrm{CL}}^{\mathrm{a}}(\boldsymbol{e}_{(k)})]^{\mathrm{T}}\boldsymbol{P}[\boldsymbol{E}_{\mathrm{CL}}^{\mathrm{e}}(\boldsymbol{e}_{(k)}) - \boldsymbol{E}_{\mathrm{CL}}^{\mathrm{a}}(\boldsymbol{e}_{(k)})]\\ &+2\boldsymbol{e}_{(k)}^{\mathrm{T}}\boldsymbol{M}_k^{\mathrm{T}}\boldsymbol{P}[\boldsymbol{E}_{\mathrm{CL}}^{\mathrm{e}}(\boldsymbol{e}_{(k)}) - \boldsymbol{E}_{\mathrm{CL}}^{\mathrm{a}}(\boldsymbol{e}_{(k)})],\\ \Delta V(\boldsymbol{e}_{(k)}) \leqslant& -b_3\|\boldsymbol{e}_{(k)}\|^2 + \lambda_{\max}(\boldsymbol{P})[\|\boldsymbol{N}_k\| + \phi_1]^2\\ &+2\lambda_{\max}(\boldsymbol{P})\|\boldsymbol{M}_k\|\|\boldsymbol{e}_{(k)}\|[\|\boldsymbol{N}_k\| + \phi_1].\end{aligned}$$

Let $0 < \nu < 1$, then

$$\begin{aligned}\Delta V(\boldsymbol{e}_{(k)}) \leqslant& -(1-\nu)b_3\|\boldsymbol{e}_{(k)}\|^2 - \nu b_3\|\boldsymbol{e}_{(k)}\|^2\\ &+ 2\lambda_{\max}(\boldsymbol{P})\xi[\|\boldsymbol{N}_k\| + \phi_1]\|\boldsymbol{e}_{(k)}\|\\ &+ \lambda_{\max}(\boldsymbol{P})[\|\boldsymbol{N}_k\| + \phi_1]^2.\end{aligned}$$

Solving the following inequality for a positive solution

$$\nu b_3\|\boldsymbol{e}_{(k)}\|^2 - 2\lambda_{\max}(\boldsymbol{P})\xi[\|\boldsymbol{N}_k\| + \phi_1]\|\boldsymbol{e}_{(k)}\| \\ - \lambda_{\max}(\boldsymbol{P})[\|\boldsymbol{N}_k\| + \phi_1]^2 \geqslant 0,$$

and defining

$$b_5 = \lambda_{\max}(\boldsymbol{P})\xi + \sqrt{\lambda_{\max}^2(\boldsymbol{P})\xi^2 + \lambda_{\max}(\boldsymbol{P})\nu b_3}$$

and $\mu \triangleq \dfrac{b_5(\|\boldsymbol{N}_k\| + \phi_1)}{\nu b_3}$ yield

$$\|\boldsymbol{e}_{(k)}\| \geqslant \mu.$$

Then,

$$\Delta V(\boldsymbol{e}_{(k)}) \leqslant -(1-\nu)b_3\|\boldsymbol{e}_{(k)}\|^2, \ \ \forall \|\boldsymbol{e}_{(k)}\| \geqslant \mu.$$

From (47), we obtain $b_2\mu^2 < b_1\delta^2$ and since $b_1 \leqslant b_2$ this in turn implies $\mu < \delta$. The remainder of the proof follows similar arguments as in the proof of [19, Theorem 4.18]. Define $D_\mu = \{\boldsymbol{e} \,|\, \|\boldsymbol{e}\| \leqslant \mu\}$, $D_\delta = \{\boldsymbol{e} \,|\, \|\boldsymbol{e}\| \leqslant \delta\}$, $\varGamma_\mu = \{\boldsymbol{e} \in D_\delta \,|\, V(\boldsymbol{e}) \leqslant b_2\mu^2\}$, and $\varGamma_\delta = \{\boldsymbol{e} \in D_\delta \,|\, V(\boldsymbol{e}) \leqslant b_1\delta^2\}$, then

$$D_\mu \subset \varGamma_\mu \subset \varGamma_\delta \subset D_\delta.$$

A solution starting either in $\varGamma_\delta$ or $\varGamma_\mu$ cannot leave the set, because $\Delta V(\boldsymbol{e}_{(k)})$ is negative for all $\|\boldsymbol{e}_k\| \geqslant \mu$ and $\delta > \mu$. Indeed, from (49), $b_2\|\boldsymbol{e}_{(k_0)}\|^2 \leqslant b_1\delta^2$, then $\boldsymbol{e}_{(k_0)} \in \varGamma_\delta$ and $\boldsymbol{e}_{(k)} \in \varGamma_\delta$, $\forall k \geqslant k_0$. Similarly, taking into account that $\varGamma_\mu \subset \{\boldsymbol{e} \in D_\delta \,|\, b_1\|\boldsymbol{e}\|^2 \leqslant b_2\mu^2\}$, for a solution starting in $\varGamma_\mu$ we have $\boldsymbol{e}_{(k)} \in \varGamma_\mu, \forall k \geqslant k_0$, and (51) is satisfied.

It remains to establish that a solution starting in $\varGamma_\delta$ must enter $\varGamma_\mu$ in finite time. In the set $\{\varGamma_\delta - \varGamma_\mu\}$,

$$\Delta V(\boldsymbol{e}_{(k)}) \leqslant -(1-\nu)b_3\|\boldsymbol{e}_{(k)}\|^2 \leqslant -\frac{(1-\nu)b_3}{b_2}V(\boldsymbol{e}_{(k)}).$$

By [19, Lemmas 3.4 and 4.4] and [23, Theorem 8], $V(\boldsymbol{e}_{(k)})$ satisfies

$$V(\boldsymbol{e}_{(k)}) \leqslant V(\boldsymbol{e}_{(k_0)})e^{-(1-\nu)\frac{b_3}{b_2}(k-k_0)} \\ \leqslant b_2\|\boldsymbol{e}_{(k)}\|^2 e^{-(1-\nu)\frac{b_3}{b_2}(k-k_0)}.$$

From (44),

$$\|\boldsymbol{e}_{(k)}\|^2 \leqslant \frac{V(\boldsymbol{e}_{(k)})}{b_1} \leqslant \frac{b_2}{b_1}\|\boldsymbol{e}_{(k)}\|^2 e^{-(1-\nu)\frac{b_3}{b_2}(k-k_0)}.$$

Hence there is a finite time step k_1 after which $\boldsymbol{e}_{(k)} \in \varGamma_\mu, \forall k \geqslant k_1$, and so (50) and (51) are established. □

We point out that in the proof of this theorem, all the relevant matrices are evaluated using the state of the *exact* model. This is a standard approach presented in [19, Chapter 9].

Remark 4 For $\boldsymbol{P} = \alpha\boldsymbol{I}$, we have $b_1 = b_2 = \alpha$, $b_3 = \alpha(1-\xi^2)$, $b_5 = \alpha(\xi + \sqrt{\xi^2 + \nu(1-\xi^2)})$ and $\Delta V(\boldsymbol{e}_{(k)}) \leqslant -(1-\nu)\alpha(1-\xi^2)\|\boldsymbol{e}_{(k)}\|^2$ for $\forall \|\boldsymbol{e}_{(k)}\| \geqslant \dfrac{(\|\boldsymbol{N}_k\| + \phi_1)(\xi + \sqrt{\xi^2 + \nu(1-\xi^2)})}{\nu(1-\xi^2)}$. Equations (47)–(49), and the expressions for C_2, φ and B can be modified accordingly. Note that to satisfy equations (47)–(49), δ should be chosen sufficiently large. However increasing δ leads to conservative bounds. Since the selection of δ is affected by the ratios (b_3/b_5) and (b_1/b_2), to reduce conservatism making $b_1 = b_2$, i.e., $\boldsymbol{P} = \alpha\boldsymbol{I}$ is a good choice.

As a result, the stability of the exact closed-loop discrete model, $\boldsymbol{E}^{\mathrm{e}}_{\mathrm{CL}}(\boldsymbol{e}_{(k)})$, is determined by (42), (43), (47) and (48).

Note that it is always difficult to get tight bounds using Lyapunov functions to establish regions of stability. To obtain less conservative results in practice, we propose using Lyapunov transformation for the closed-loop error equation (40) as follows:

Let $\boldsymbol{L}_{(k)}$ denote a time varying square non-singular matrix such that $\boldsymbol{L}_{(k)}$ and its inverse are uniformly bounded. We can write

$$\tilde{\boldsymbol{e}}_{(k+1)} = \boldsymbol{L}_{(k+1)}\boldsymbol{e}_{(k+1)}. \tag{52}$$

The linear system (40) can then be written in an equivalent representation using (52) noting that $\boldsymbol{e}_{(k)} = \boldsymbol{L}^{-1}_{(k)}\tilde{\boldsymbol{e}}_{(k)}$ as

$$\begin{aligned}\tilde{\boldsymbol{e}}_{(k+1)} &= \boldsymbol{L}_{(k+1)}\boldsymbol{M}_k\boldsymbol{e}_{(k)} + \boldsymbol{L}_{(k+1)}\boldsymbol{N}_k \\ &= \boldsymbol{L}_{(k+1)}\boldsymbol{M}_k\boldsymbol{L}^{-1}_{(k)}\tilde{\boldsymbol{e}}_{(k)} + \boldsymbol{L}_{(k+1)}\boldsymbol{N}_k \\ &= \tilde{\boldsymbol{M}}_k\tilde{\boldsymbol{e}}_{(k)} + \tilde{\boldsymbol{N}}_k.\end{aligned} \tag{53}$$

Since $\boldsymbol{L}_{(k)}$ is a Lyapunov transformation, it preserves the properties of stability, instability, and asymptotic stability; and in this sense, (40) and (53) are equivalent representations. In addition, if $\boldsymbol{M}_k$ is periodic and has a non-zero determinant for all k, then there is a Lyapunov transformation such that $\tilde{\boldsymbol{M}}_k$ is time invariant and hence the stability properties are determined by the eigenvalues of $\tilde{\boldsymbol{M}}_k$. (For further results on time-varying Lyapunov transformations, refer to [24].)

4 Numerical verification

Numerical simulation is performed to verify the stability analysis of the standard discrete-time TDC.

4.1 Case 1: the first-order nonlinear system

In this section, the first order nonlinear system $\dot{x}_{(t)} = x^3_{(t)} + \sin x_{(t)} + 5u_{(t)}$ is considered as a plant, whilst its linearised model was used to illustrate the example in Section 2.3. The result of the proposed stability criteria is particularly examined when different sampling frequencies as well as trajectories are assigned to the controller, compared with the actual stability region.

Here, $g_p(x) = 5$, which is unknown to a control designer. Therefore the gain of TDC, denoted as $\bar{g}$, has to be properly chosen as suggested by (5) [16]. For the aforementioned plant, the TDC (4) is implemented in the standard discrete form (9), given by

$$u_{(k)} = u_{(k-1)} + \bar{g}^{-1}[-\dot{x}_{(k-1)} + A_{\rm m}x_{(k)} + (\dot{x}_{{\rm d}(k)} - A_{\rm m}x_{{\rm d}(k)})],$$

where u denotes the input, $A_{\rm m}$ denotes the reference model parameter, x denotes the state, and $x_{\rm d}$ denotes the desired trajectory (Note that $B_{\rm m}R_{(k)} = \dot{x}_{{\rm d}(k)} - A_{\rm m}x_{{\rm d}(k)}$, [25]). $A_{\rm m} = -40$ is set in the simulation.

In this paper, the proposed stability criteria, (42), (43), (47) and (48), are verified under different sampling time conditions: $T = 0.01$, 0.005, and 0.001 s. Moreover, unlike existing literature on stability of TDC, we analyse the impact of the reference trajectory on the overall stability using the proposed method. The reference trajectories used in simulations are shown in Fig. 1; the 5th order polynomial trajectory is

$$x_{{\rm d}(t)} = \begin{cases} 10t^3 - 15t^4 + 6t^5, & t \leqslant 1\,{\rm s}, \\ 1, & t > 1\,{\rm s}, \end{cases} \quad (54)$$

and two sinusoidal trajectories are

$$x_{{\rm d}(t)} = \begin{cases} \sin(\frac{1}{2}t), & (55) \\ \sin(2t). & (56) \end{cases}$$

For consistency of results, all necessary parameters of the proposed stability are set to the same values as for $\boldsymbol{P} = \boldsymbol{I}$, $\delta = 0.5\sqrt{2}$, $\nu = 0.99$, and $k_{\rm s} = 100$. Note that evaluating ϕ_1 in Lemma 2 requires the knowledge of the exact discrete-time model of the nonlinear system. In this simulation verification, it is acquired by numerically solving the differential equation; for example, a differential equation solver *ode45* in Matlab® is widely accepted for the accuracy, which implements a Runge-Kutta(4, 5) formula, also known as the Dormand-Prince pair [26].

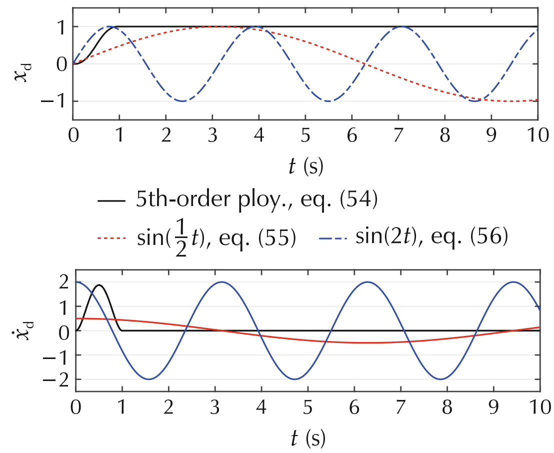

Fig. 1 The desired trajectories $x_{{\rm d}(t)}$ and $\dot{x}_{{\rm d}(t)}$ in simulations.

Fig. 2 depicts the stable range of values for $\bar{g}$ at $T = 0.01$ s when the system is controlled to track the sinusoidal reference (56). The proposed sufficient stability criterion (43) and (48) are respectively evaluated with respect to the change of $\bar{g}$; this reveals that the gains in the range of $2.998 \leqslant \bar{g} \leqslant 77$ guarantee stable tracking of the reference $x_{{\rm d}(t)} = \sin(2t)$.

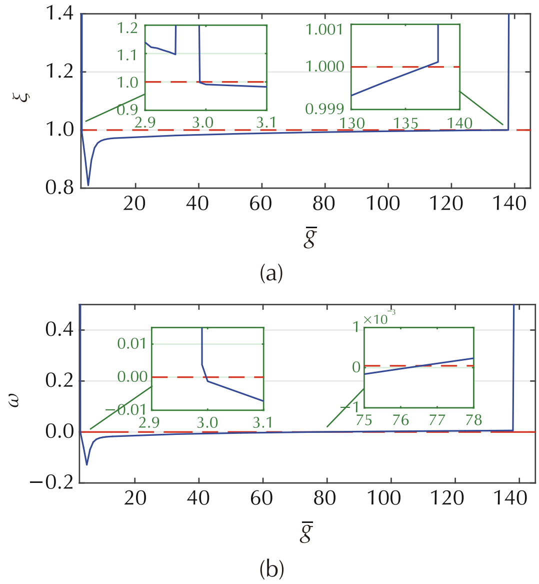

Fig. 2 The evaluation of the proposed stability criterion ξ and ω as a function of $\bar{g}$ for a sampling time interval $T = 0.01$ s with the reference $x_{\rm d} = \sin(2t)$. (a) $\bar{g}$ vs. ξ; $0 < \xi < 1$. (b) $\bar{g}$ vs. ω; $\omega < 0$.

Through the same procedure for other references (54) and (55), and sample times $T = 0.005$ s and 0.001 s, one can obtain the range of $\bar{g}$ satisfying the proposed stability criterion. Results are summarised in Table 1, where the gain sets of the actual stability criterion are found by trial and error in numerical experiments.

Table 1 Range of $\bar{g}$ meets sufficient stability criteria for different sampling time and desired trajectory.

(a) The 5th order polynomial $x_{d(t)}$.

Sampling time T	$\bar{g}$ range: Proposed method	$\bar{g}$ range: Actual values
0.010	**[2.991, 82]**	[2.960, 138]
0.005	**[2.745, 169]**	[2.728, 279]
0.001	**[2.554, 780]**	[2.550, 1409]

(b) $x_{d(t)} = \sin(0.5t)$.

Sampling time T	$\bar{g}$ range: Proposed method	$\bar{g}$ range: Actual values
0.010	**[2.990, 119]**	[2.972, 217]
0.005	**[2.794, 231]**	[2.736, 437]
0.001	**[2.690, 1055]**	[2.548, 2190]

(c) $x_{d(t)} = \sin(2t)$.

Sampling time T	$\bar{g}$ range: Proposed method	$\bar{g}$ range: Actual values
0.010	**[2.998, 77]**	[2.972, 201]
0.005	**[2.799, 144]**	[2.736, 390]
0.001	**[2.695, 557]**	[2.548, 2010]

As seen in Table 1, the lower bounds of the proposed criterion are close to the actual ones, while its upper bounds are rather conservative. From a close investigation of the case shown in Fig. 2, one can notice that the condition $\omega < 0$ gives more conservative bounds of $\bar{g}$ than those from $0 < \xi < 1$. It is mainly because ω is determined by δ as seen in (48), which is specified as the maximum error norm bound (49); in other words, by setting δ, one can effectively define the allowable maximum error range regarding the stability.

The results presented in Table 1, i.e., the upper and lower bound values of $\bar{g}$, are verified by the simulations of the standard discrete TDC, as shown in Fig. 3, for $T = 0.001$ s with the 5th order polynomial trajectory, $T = 0.005$ s with $x_d = \sin(0.5t)$, and $T = 0.01$ s with $x_d = \sin(2t)$. (Since other six cases present the similar results, they are omitted for the brevity of the paper.) This illustrates that the system is stable and error norms $\|\boldsymbol{e}\|$ are much less than the specified error norm bound δ.

Note the conventional stability criterion (5) only gives the lower bound of the gain as $\bar{g} > 2.5$. Whereas, it is clearly seen that the proposed stability criterion provides both upper and lower bounds that depend on the sampling time T as well as the reference x_d. The stable range of the gain increases as the size of sample time decreases under the same reference; in addition, as the frequency of the sinusoidal trajectory increases, the stable gain range decreases. These results are consistent with observed experimental results in actual TDC systems.

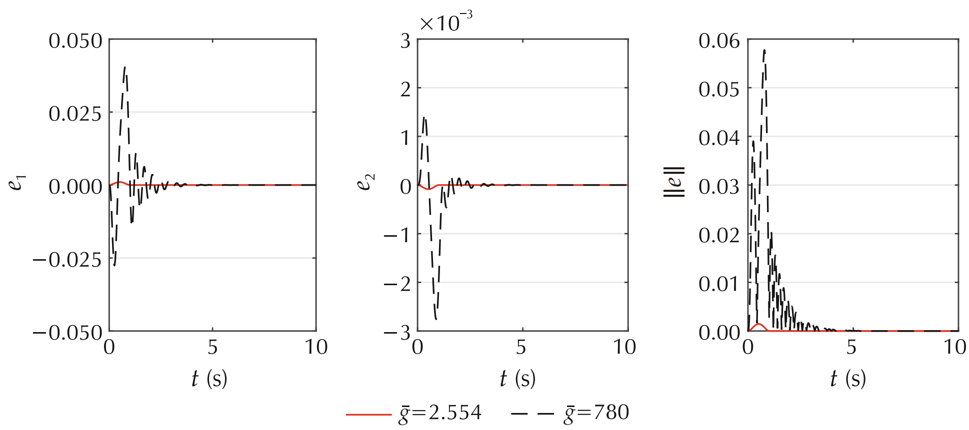

(a)

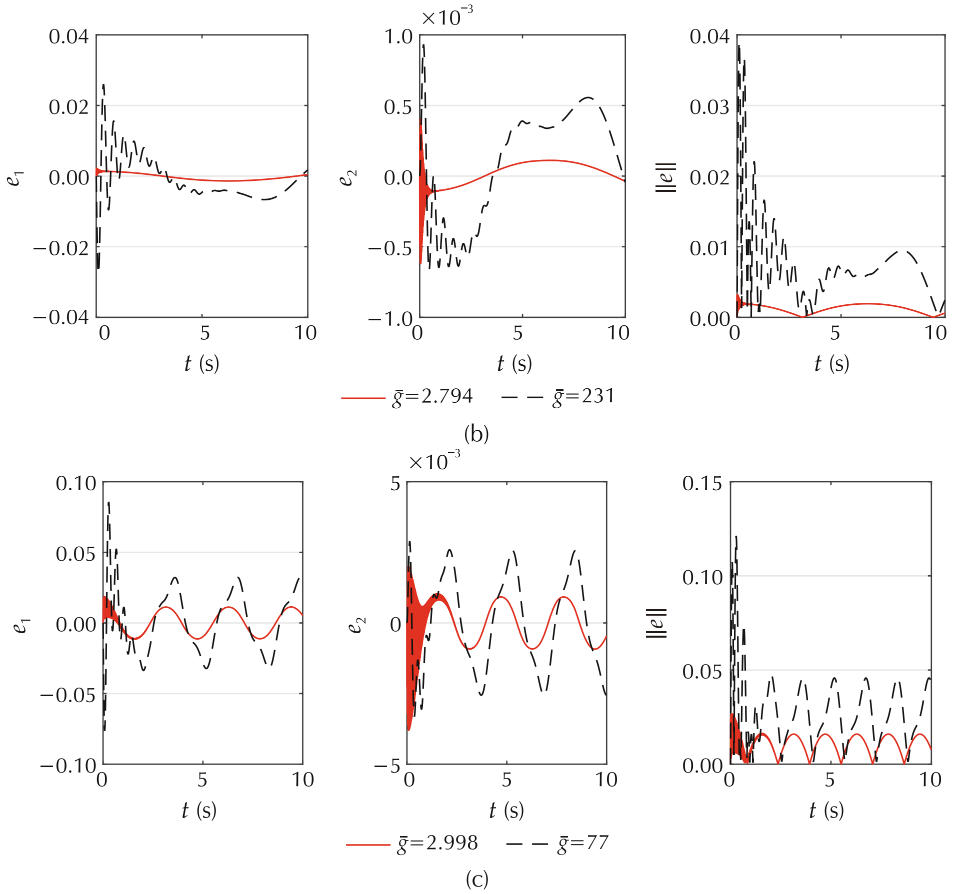

Fig. 3 The error responses $e_1 = x - x_{\mathrm{m}}$, $e_2 = (u - u_{\mathrm{m}})/k_{\mathrm{s}}$, and the error norm $\|e\|$, where the red-solid and black-dashed lines respectively correspond to the lower and upper bounds of $\bar{g}$ from the proposed stability criteria shown in Table 1. (a) $T = 0.001$ s under the 5th order polynomial trajectory, equation (54). (b) $T = 0.005$ s under the trajectory $\sin(\frac{1}{2}t)$, equation (55). (c) $T = 0.010$ s under the trajectory $\sin(2t)$, equation (56).

4.2 Case 2: a two-link manipulator

In this section, dynamic simulations for a two degrees-of-freedom manipulator are performed to validate the proposed stability analysis of the standard discrete TDC as an example of a practical nonlinear system application. Fig. 4 illustrates the two-link manipulator described by the following dynamics:

$$\boldsymbol{\tau} = \boldsymbol{M}(\boldsymbol{\theta})\ddot{\boldsymbol{\theta}} + \boldsymbol{C}(\dot{\boldsymbol{\theta}}, \boldsymbol{\theta}) + \boldsymbol{g}(\boldsymbol{\theta}), \tag{57}$$

where $\boldsymbol{\tau} \in \mathbb{R}^2$ denotes the joint torque vector, $\boldsymbol{\theta} \in \mathbb{R}^2$ denotes the joint angle vector, $\boldsymbol{M}(\boldsymbol{\theta})$ denotes the manipulator inertia matrix, $\boldsymbol{C}(\dot{\boldsymbol{\theta}}, \boldsymbol{\theta})$ denotes the centrifugal and Coriolis torque matrix, and $\boldsymbol{g}(\boldsymbol{\theta})$ denotes the gravitational torque vector, while their elements are given as

$$M_{11} = m_1 l_{\mathrm{c}1}^2 + m_2(l_1^2 + l_{\mathrm{c}2}^2 + 2l_1 l_{\mathrm{c}2}\cos\theta_2) + I_1 + I_2,$$
$$M_{12} = M_{21} = m_2(l_{\mathrm{c}2}^2 + l_1 l_{\mathrm{c}2}\cos\theta_2) + I_2,$$
$$M_{22} = m_2 l_{\mathrm{c}2}^2 + I_2,$$
$$C_1 = -m_2 l_1 l_{\mathrm{c}2}\sin\theta_2(2\dot{\theta}_1\dot{\theta}_2 + \dot{\theta}_1^2),$$
$$C_2 = m_2 l_1 l_{\mathrm{c}2}\sin\theta_2\dot{\theta}_1^2,$$
$$g_1 = \{(m_1 l_{\mathrm{c}1} + m_2 l_1)\cos\theta_1 + m_2 l_{\mathrm{c}2}\cos(\theta_1 + \theta_2)\}\mathrm{g},$$
$$g_2 = m_2 l_{\mathrm{c}2}\cos(\theta_1 + \theta_2)\mathrm{g},$$

where $(m_1, l_1, l_{\mathrm{c}1}, I_1)$, $(m_2, l_2, l_{\mathrm{c}2}, I_2)$ denote the mass, link lengths, position of the centre of mass, and the moment of inertia of links 1 and 2, respectively. The system can be expressed in the nonlinear system structure (1) and (2) as follows:

$$\boldsymbol{x} = \begin{bmatrix} \boldsymbol{\theta} \\ \dot{\boldsymbol{\theta}} \end{bmatrix}, \quad \boldsymbol{f}(\boldsymbol{x}) = \begin{bmatrix} \dot{\boldsymbol{\theta}} \\ -\boldsymbol{M}(\boldsymbol{\theta})^{-1}(\boldsymbol{C}(\dot{\boldsymbol{\theta}}, \boldsymbol{\theta}) + \boldsymbol{g}(\boldsymbol{\theta})) \end{bmatrix},$$
$$\boldsymbol{g}(\boldsymbol{x}) = \begin{bmatrix} \boldsymbol{0}_2 \\ \boldsymbol{M}(\boldsymbol{\theta})^{-1} \end{bmatrix}, \quad \boldsymbol{u} = \boldsymbol{\tau}.$$

The following parameter values are selected for simulations: $m_1 = m_2 = 1\,\text{kg}$, $l_1 = l_2 = 1\,\text{m}$, $l_{c1} = l_{c2} = 1/2\,\text{m}$, $I_1 = I_2 = 1/12\,\text{kg}\cdot\text{m}^2$, and $\text{g} = 9.81\,\text{m/s}^2$.

The reference model is chosen as

$$A_\text{m} = \begin{bmatrix} \mathbf{0}_2 & \boldsymbol{I}_2 \\ -\omega_n^2\boldsymbol{I}_2 & -2\zeta_n\omega_n\boldsymbol{I}_2 \end{bmatrix},\quad B_\text{m} = \begin{bmatrix} \mathbf{0}_2 \\ \omega_n^2\boldsymbol{I}_2 \end{bmatrix},$$

where ω_n and ζ_n denote the desired natural frequency and damping ratio of the manipulator system, respectively. In the simulation, $\omega_n = 10\,\text{rad/s}$ and $\zeta_n = 0.707$ are used for all joints.

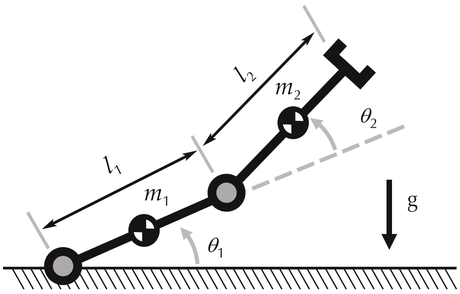

Fig. 4 Schematic diagram of a two-link manipulator.

The gain of TDC, $\bar{g}^+$, is set to a constant matrix, often determined by a nominal value of $g(x)$ [16]. Here, we consider the following gain matrix:

$$\bar{g}^+ = \beta[\mathbf{0}_2 \;\; \bar{\boldsymbol{M}}],$$

where β is a positive scalar to scale the gain value and $\bar{\boldsymbol{M}}$ is a constant matrix selected as $\bar{\boldsymbol{M}} = \begin{bmatrix} \frac{5}{8} & \frac{1}{8} \\ \frac{1}{8} & \frac{1}{8} \end{bmatrix}$, which is the inertia matrix evaluated at $\theta_2 = \dfrac{\pi}{2}$ rad and scaled down by $\dfrac{3}{8}$. The single scale gain β is introduced for simplicity in the stability simulations presented in this paper; in general, the gain for each joint can be independently selected. Fig. 5 presents the tracking control result of the two-link manipulator by standard discrete TDC, where the sampling time is set to $T = 0.005\,\text{s}$ and the gain scale $\beta = 1$.

The proposed stability criteria, (42), (43), (47), and (48), are then determined under the sampling time condition of $T = 0.005\,\text{s}$, when two joints are commanded to track the same 5th order polynomial trajectory for ten seconds as shown in Fig. 5 (a). All necessary parameters of the proposed stability are set to the same values as for $\boldsymbol{P} = \boldsymbol{I}$, $\delta = 4.7\text{E}4$, $\nu = 0.99$, and $k_\text{s} = 100$.

Fig. 6 then shows the analysis result regarding the stable range of gain values represented by the scale β. The proposed sufficient stability criterion $0 < \xi < 1$, given by (43), and $\omega < 0$, given by (48), are respectively evaluated with respect to the change of β; this reveals that the determined gains in the range of $0.2057 < \beta < 1.2873$ guarantee stable tracking of the given trajectory. Those lower- and upper-bound gains obtained from the stability analysis are evaluated as shown in Fig. 7. Note that the conventional stability criterion (5) gives $0 < \beta < 0.8610$, regardless of the sampling time and the trajectory.

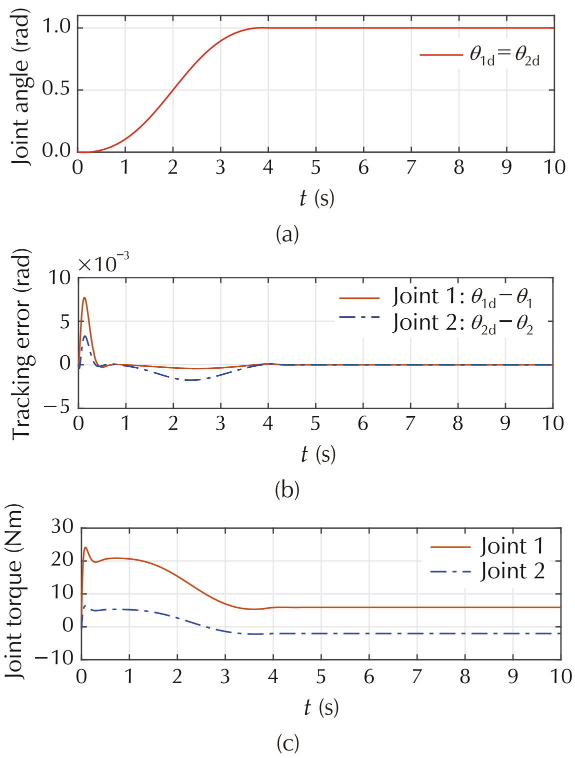

Fig. 5 Simulation of standard disrecte TDC for the two link manipulator when $T = 0.005\,\text{s}$ and gain scale $\beta = 1$ are set. (a) Desired trajectory. (b) Tracking error. (c) Control signal.

Compared to the result controlled with nominal stable gain shown in Fig. 5, one can observe that the responses and control inputs with lower-bound gain exhibit slowly decaying oscillations and the tracking performance is rather poor; and for the upper-bound gain case, while the error responses appear to be stable, the control torques start to oscillate. As found by changing gains by trial and error in simulations, the actual instability occurs when the gain is $\beta < 0.1406$ or $\beta > 1.6015$. Thus, it is confirmed that the proposed stability criteria properly provide sufficient condition, and this trend is also consistent to the results shown in Case 1. Therefore, we verify that the proposed stability criterion of standard discrete TDC can be applied to the practical two-link manipulator system and can offer the stable region of the gain.

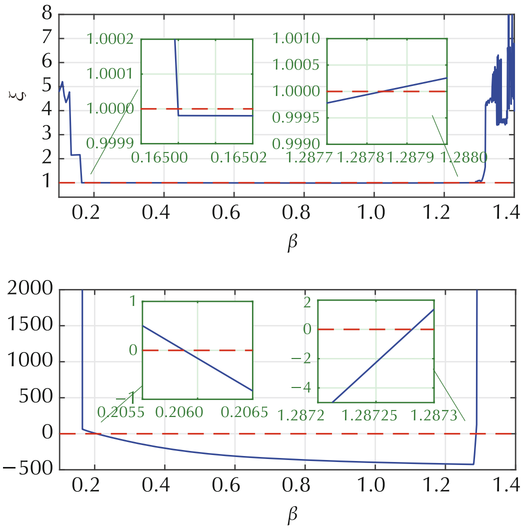

Fig. 6 The proposed stability criterion ξ and ω evaluation: x-axes are the gain scale β, while y-axis of the upper plot is ξ, equation (43) and that of lower plot is ω, equation (48).

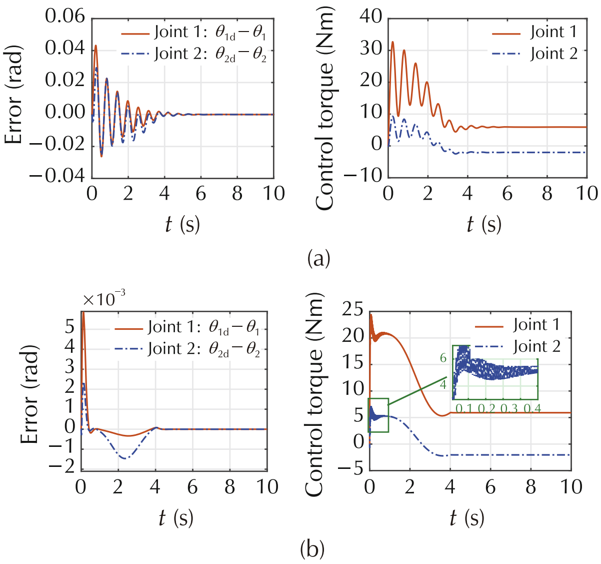

Fig. 7 The tracking error responses and control torques of two joints for lower- and upper-bound gains obtained from the proposed stability analysis. (a) Lower bound gain $\beta = 0.2060$. (b) Upper bound gain $\beta = 1.2873$.

5 Conclusions

In this paper, we have theoretically investigated the stability criteria for a nonlinear system under the standard form of discrete-time time delay control (TDC). An approximate discrete-time model of the nonlinear system under the standard TDC is derived and sufficient stability criteria are then proposed. Additionally, tight bounds in the sufficient condition are provided by exploiting Lyapunov transformations. These criteria have been verified by simulation results offering insight into finding the impact of the sampling period, desired and reference model dynamics trajectory on the actual closed-loop system stability.

References

[1] R. Morgan, U. Ozguner. A decentralized variable structure control algorithm for robotic manipulators. *IEEE Journal on Robotics and Automation*, 1985, 1(1): 57 – 65

[2] K. Youcef-Toumi, O. Ito. Controller design for systems with unknown nonlinear dynamics. *Proceedings of the American Control Conference*, Minneapolis: IEEE, 1987: 836 – 845.

[3] T. C. Hsia. On a simplified joint controller design for robot manipulators. *Proceedings of the IEEE Conference on Decision and Control*, Los Angeles: IEEE, 1987: 1024 – 1025.

[4] T. C. Hsia. A new technique for robust control of servo systems. *IEEE Transactions on Industrial Electronics*, 1989, 36(1): 1 – 7.

[5] P. H. Chang, D. S. Kim, K. C. Park. Robust force/position control of a robot manipulator using time-delay control. *Control Engineering Practice*, 1995, 3(9): 1255 – 1264.

[6] H-S. Kim, K-H. Kim, M-J. Youn. On-line dead-time compensation method based on time delay control. *IEEE Transactions on Control Systems Technology*, 2003, 11(2): 279 – 285.

[7] S. E. Talole, A. Ghosh, S. B. Phadke. Proportional navigation guidance using predictive and time delay control. *Control Engineering Practice*, 2006, 14(12): 1445 – 1453.

[8] R. P. Kumar, C. S. Kumar, D. Sen, et al. Discrete time-delay control of an autonomous underwater vehicle: Theory and experimental results. *Ocean Engineering*, 2009, 36(1): 74 – 81.

[9] P. H. Chang, J. H. Jung. A systematic method for gain selection of robust PID control for nonlinear plants of second-order controller canonical form. *IEEE Transactions on Control Systems Technology*, 2009, 17(2): 473 – 483.

[10] G. R. Cho, P. H. Chang, S. H. Park, et al. Robust tracking under nonlinear friction using time-delay control with internal model. *IEEE Transactions on Control Systems Technology*, 2009, 17(6): 1406 – 1414.

[11] J. Lee, C. Yoo, Y-S. Park, et al. An experimental study on time delay control of actuation system of tilt rotor unmanned aerial vehicle. *Mechatronics*, 2012, 22(2): 184 – 194.

[12] J. H. Lee, B. J. Kim, J. S.Kim, et al. Time-delay control of ionic polymer metal composite actuator. *Smart Materials and Structures*, 2015, 24(4): DOI https://doi.org/10.1088/0964-1726/24/4/047002.

[13] J. Kim, H. Joe, S-C. Yu, et al. Time-delay controller design for position control of autonomous underwater vehicle under disturbances. *IEEE Transactions on Industrial Electronics*, 2016, 63(2): 1052 – 1061.

[14] B. U. Rehman, M. Focchi, J. Lee, et al. Towards a multi-legged mobile manipulator. *Proceedings of the IEEE International Conference on Robotics and Automation*, Stockholm: IEEE, 2016: 3618 – 3624.

[15] K. Youcef-Toumi, O. Ito. A time delay controller for systems with unknown dynamics. *Journal of Dynamic Systems, Measurement, and Control*, 1990, 112(1): 133 – 142.

[16] K. Youcef-Toumi, S-T. Wu. Input/output linearization using time delay control. *Journal of Dynamic Systems, Measurement, and Control*, 1992, 114(1): 10 – 19.

[17] J. H. Jung, P. H. Chang, D. Stefanov. Discretisation method and stability criteria for non-linear systems under discrete-time time delay control. *IET Control Theory & Applications*, 2011, 5(11): 1264 – 1276.

[18] J. Lee, G. A. Medrano-Cerda, J. H. Jung. Corrections for Discretisation method and stability criteria for non-linear systems under discrete-time time delay control. *IET Control Theory & Applications*, 2016, 10(14): 1751 – 1754.

[19] H. K. Khalil. *Nonlinear Systems*. 3rd ed. Upper Saddle River: Prentice Hall, 2002.

[20] S. Dayal. A converse of Taylor's theorem for functions on Banach spaces. *Proceedings of the American Mathematical Society*, 1977, 65(2): 265 – 273.

[21] B. Friedland. *Control System Design – An Introduction to State Space Methods*. New York: McGraw-Hill, 1989.

[22] D. Nešić, A. R. Teel, P. V. Kokotović. Sufficient conditions for stabilization of sampled-data nonlinear systems via discrete-time approximations. *Systems & Control Letters*, 1999, 38(4): 259 – 270.

[23] D. Nešićc, A. R. Teel, E. D. Sontag. Formulas relating KL stability estimates of discrete-time and sampled-data nonlinear systems. *Systems & Control Letters*, 199, 38(1): 49 – 609.

[24] F. R. Gantmacher. *The Theory of Matrices*. New York: Chelsea Publishing Company, 1959.

[25] P. H. Chang, J. W. Lee. A model reference observer for time-delay control and its application to robot trajectory control. *IEEE Transactions on Control Systems Technology*, 1996, 4(1): 2 – 10.

[26] J. R. Dormand, P. J. Prince. A family of embedded Runge-Kutta formulae. *Journal of Computational and Applied Mathematics*, 1980, 6(1): 19 – 26.

Appendix

A Taylor series expansion of $f(\chi_i)$ and $g(\chi_i)u_{(k-1)}$

The first order Taylor series of $f(\chi_i)$ is given as

$$f(\chi_i) \approx f(\chi_0) + F(\chi_0)(\chi_i - \chi_0). \tag{a1}$$

where F denotes the partial derivatives in terms of χ such that $[F(\chi_0)]_{a,b} = \dfrac{\partial [f]_a}{\partial [\chi]_b}(\chi_0)$ for $a, b = 1, \dots, n$. Similarly, the first order Taylor series of $g(\chi_i)u_{(k-1)}$ is written as

$$g(\chi_i)u_{(k-1)} \approx g(\chi_0)u_{(k-1)} + G(\chi_0, u_{(k-1)})(\chi_i - \chi_0), \tag{a2}$$

where $[Gx(\chi_0, u_{(k-1)})]_{a,b} = \sum\limits_{j=1}^{p} \dfrac{\partial g_{a,j}(\chi_0)}{\partial \chi_b} u_{j(k)}$.

B Taylor expansion residual

$$[O_1(x_{(k)}, x_{\mathrm{m}(k)})]_a = \frac{1}{2}\sum_{i,j=1}^{a} \frac{\partial^2 [f(x_{q(k)})]_a}{\partial [x]_i \partial [x]_j}[e_{1(k)}]_i [e_{1(k)}]_j, \tag{a3}$$

where $[\,\cdot\,]_a$ denotes the ath element of "$\cdot$" for $a = 1, \dots, n$ and $x_{q(k)}$ is a certain point in the line joining $x_{(k)}$ and $x_{\mathrm{m}(k)}$. Hereinafter, for brevity, $O_1(x_{(k)}, x_{\mathrm{m}(k)})$ will be written as $O_{1(k)}$.

C Detailed expression of matrices in (36) & (37)

$$E_1 = -\bar{g}^{+}A_{\mathrm{m}}/k_{\mathrm{s}} \ \in \mathbb{R}^{p\times n},$$

$$\begin{cases} S_1 = I_n + C_k g_k \bar{g}^{+} A_{\mathrm{m}} + C_k F(x_{\mathrm{m}(k)}) \ \in \mathbb{R}^{n\times n}, \\ S_2 = -C_k g_k \bar{g}^{+} F(x_{\mathrm{m}(k-1)}) \ \in \mathbb{R}^{n\times n}, \\ S_3 = k_{\mathrm{s}} C_k g_k \bar{g}^{+}(\bar{g} - g_{(k-1)}) = k_{\mathrm{s}} C_k g_k (I_n - \bar{g}^{+} g_{(k-1)}) \\ \quad \in \mathbb{R}^{n\times p}, \\ S_4 = -\bar{g}^{+} F(x_{\mathrm{m}(k)})/k_{\mathrm{s}} \in \mathbb{R}^{p\times n}, \\ S_5 = \bar{g}^{+}(\bar{g} - g_k) = (I_n - \bar{g}^{+} g_k) \in \mathbb{R}^{p\times p}, \end{cases}$$

$$\begin{cases} Q_1 = C_k \in \mathbb{R}^{n}, \\ Q_2 = -C_k g_k \bar{g}^{+} \in \mathbb{R}^{n}, \\ Q_3 = C_k - (D_1 - I_n)A_{\mathrm{m}}^{-1}(I_n - \bar{g}\bar{g}^{+}) \in \mathbb{R}^{n}, \\ Q_4 = -(D_1 - I_n)A_{\mathrm{m}}^{-1}\bar{g}\bar{g}^{+} \in \mathbb{R}^{n}, \\ Q_5 = C_k g_k - (D_1 - I_n)A_{\mathrm{m}}^{-1}\bar{g} \in \mathbb{R}^{n}, \\ Q_6 = C_k g_k \bar{g}^{+}[g(x_{\mathrm{m}(k-1)}) - g_{(k-1)}] \\ \qquad -(D_1 - I_n)A_{\mathrm{m}}^{-1}\bar{g}\bar{g}^{+}[g(x_{\mathrm{m}(k-1)}) - \bar{g}] \in \mathbb{R}^{n}, \\ Q_7 = -\bar{g}^{+}/k_{\mathrm{s}} \in \mathbb{R}^{p}, \\ Q_8 = \bar{g}^{+}[g(x_{\mathrm{m}(k)}) - g_k]/k_{\mathrm{s}} \in \mathbb{R}^{p}. \end{cases}$$

Note that all these matrices are functions of $x_{(k)}$, $x_{\mathrm{m}(k)}$, $x_{(k-1)}$, $x_{\mathrm{m}(k-1)}$ and depend on the sampling time interval T. This is illustrated in Section 4 with numerical simulations.

Jinoh LEE received the B.Sc. degree in Mechanical Engineering from Hanyang University, Seoul, South Korea, in 2003 (awarded Summa Cum Laude), and the M.Sc. and Ph.D. degrees in Mechanical Engineering from the Korea Advanced Institute of Science and Technology, Daejeon, South Korea, in 2012. He is currently a Research Scientist at the Department of Advanced Robotics, Istituto Italiano di Tecnologia (IIT), Genoa, Italy, where he held postdoctoral researcher position from 2012 to 2017. His professional is about robotics and control engineering, which include manipulation of highly redundant robots such as dual-arm and humanoids, robust control of nonlinear systems and compliant robotic system control for safe human-robot interaction. E-mail: jinoh.lee@iit.it.

Gustavo A. MEDRANO-CERDA received the B.Sc. degree in Electro-Mmechanical Engineering from the Universidad Nacional Autonoma de Mexico in 1977, and the M.Sc. and Ph.D. degrees in Control Systems from Imperial College, London, in 1979 and 1982, respectively. From 1982 to 1985 he was an associate professor at the Division de Estudios de Postgrado, Facultad de Ingenieria, Universidad Nacional Autonoma de Mexico. From 1985 to 1986

he was a research fellow at the Department of Engineering, University of Warwick. From 1986 to 2002 he was a lecturer at the Department of Electronic and Electrical Engineering at the University of Salford. During this period he set up the Advanced Control and Robot Locomotion Laboratory at the University of Salford. In 1999 he became a control systems consultant at Las Cumbres Observatory (formerly Telescope Technologies Ltd.) and later in 2002 he joined the company as a senior control engineer pioneering work in H-infinity control system design and implementation for astronomical telescopes. Since 2009 he has been a senior research scientist at the Advanced Robotics Department, Istituto Italiano di Tecnologia. His research interests are in the areas of robust control, adaptive control, modelling and identification, fuzzy systems and advanced robotic applications, in particular to walking robots. E-mail: gustavo.cerda@iit.it.

Je Hyung JUNG received his Ph.D. degree in Mechanical Engineering from Korea Advanced Institute of Science and Technology (KAIST), Daejeon, South Korea in 2006. He was a Postdoctoral Fellow in the Biorobotics Institute of Scuola Superiore Sant'Anna, located in Pontedera (Pisa), Italy from 2006 to 2008. Since June 2008, he has been with Tecnalia, where he is currently a senior researcher in Health Division. His research interests include modelling and control of robotic system such as multi degree of freedom manipulators and mobile robots, and design and control of rehabilitation, assistive and wearable (exoskeleton) robots, and variable stiffness materials. E-mail: jehyung.jung@tecnalia.com.